Specific involvement of postsynaptic GluN2B-containing NMDA receptors in the developmental elimination of corticospinal synapses

Takae Ohno[a], Hitoshi Maeda[a], Naoyuki Murabe[a], Tsutomu Kamiyama[a], Noboru Yoshioka[a], Masayoshi Mishina[b], and Masaki Sakurai[a,1]

[a]Department of Physiology, School of Medicine, Teikyo University, Tokyo 173-8605, Japan; and [b]Department of Molecular Neurobiology and Pharmacology, Graduate School of Medicine, University of Tokyo, Tokyo 113-8655, Japan

Edited* by Masao Ito, RIKEN Brain Science Institute, Wako, Japan, and approved July 19, 2010 (received for review July 15, 2009)

The GluN2B (GluRε2/NR2B) and GluN2A (GluRε1/NR2A) NMDA receptor (NMDAR) subtypes have been differentially implicated in activity-dependent synaptic plasticity. However, little is known about the respective contributions made by these two subtypes to developmental plasticity, in part because studies of GluN2B KO [*Grin2b*$^{-/-}$ (*2b*$^{-/-}$)] mice are hampered by early neonatal mortality. We previously used in vitro slice cocultures of rodent cerebral cortex (Cx) and spinal cord (SpC) to show that corticospinal (CS) synapses, once present throughout the SpC, are eliminated from the ventral side during development in an NMDAR-dependent manner. To study subtype specificity of NMDAR in this developmental plasticity, we cocultured Cx and SpC slices derived from postnatal day 0 (P0) animals with different genotypes [*2b*$^{-/-}$, *Grin2a*$^{-/-}$ (*2a*$^{-/-}$), or WT mice]. The distribution of CS synapses was studied electrophysiologically and with a voltage-sensitive dye. Synapse elimination on the ventral side was blocked in WT (Cx)-*2b*$^{-/-}$(SpC) pairs but not in WT(Cx)-*2a*$^{-/-}$(SpC) or *2b*$^{-/-}$(Cx)-WT(SpC) pairs. CS axonal regression was also observed through live imaging of CS axons labeled with enhanced yellow fluorescent protein (EYFP) through exo utero electroporation. These findings suggest that postsynaptic GluN2B is selectively involved in CS synapse elimination. In addition, the elimination was not blocked in *2a*$^{-/-}$ SpC slices, where Ca^{2+} entry through GluN2B-mediated CS synaptic currents was reduced to the same level as in *2b*$^{-/-}$ slices, suggesting that the differential effect of GluN2B and GluN2A in CS synapse elimination might not be explained based solely on greater Ca^{2+} entry through GluN2B-containing channels.

axon regression | synapse elimination | GluN2B (GluRε2/NR2B) | GluN2A (GluRε1/NR2A)

NMDA receptor (NMDAR)-dependent neuronal activity plays a key role in the reorganization and refinement of neuronal circuits, including ocular dominance mapping in the visual systems (1, 2) and whisker-related patterns in the barrel cortex (Cx) (3, 4). Notably, the major subunits of the heterotetrameric NMDARs commonly shift from the GluN2B [GluRε2/NR2B (2B)] subtype to the GluN2A [GluRε1/NR2A (2A)] subtype during early postnatal development (5, 6). Of the two subtypes, 2B is known to support greater Ca^{2+} influx (7, 8), making it a possible mediator of enhanced synaptic plasticity during critical periods (9–14). On the other hand, others have suggested that 2A is important for plasticity during critical periods (15–18) and that the closing of critical periods is independent of the NMDAR subtype (19). Although there have been numerous studies investigating whether periods of enhanced plasticity temporally coincide with expression of the GluN2 subunit, little is known about the direct contribution made by GluN2B to developmental plasticity, in large part because 2B KO mice die soon after birth (20).

In our previous study, we reconstructed corticospinal (CS) synapses in vitro by coculturing tissue slices obtained from the rat sensorimotor Cx and spinal cord (SpC) (21). In this in vitro CS projection model, CS synapses were widely distributed in the spinal gray matter at 7 d in vitro (DIV) but the synapses on the ventral side were subsequently eliminated through a process that was blocked by an NMDAR antagonist (22, 23). This type of synapse elimination was also seen in vivo in the rat and followed a time course similar to that seen in vitro (24), and similar elimination of synapses from ventral areas of the SpC during development has also been observed in cats (reviewed in ref. 25).

Those findings, together with the observation that the major NMDAR subunit mediating CS excitatory postsynaptic currents (EPSCs) appears to shift from 2B to 2A early during development (26), prompted us to investigate the role played by 2B in synapse reorganization during development. To accomplish this, we reconstructed our in vitro Cx-SpC slice coculture system using C57BL/6 mice and studied the time course of CS synapse elimination, testing the effect of a 2B-specific blocker. We also cocultured slices from WT and 2B or 2A KO [*Grin2b*$^{-/-}$ (*2b*$^{-/-}$) or *Grin2a*$^{-/-}$ (*2a*$^{-/-}$)] mice [heterotypic cocultures: WT(Cx)-*2b*$^{-/-}$ (SpC), WT-*2a*$^{-/-}$, and *2b*$^{-/-}$-WT] and tested for the presence of NMDAR-mediated components in CS EPSCs recorded from cultured *2b*$^{-/-}$ SpC slices. Using these heterotypic cocultures, we were able to confirm the 2B dependence of the system and determine the side on which NMDARs must be activated, Cx (presynaptic) or SpC (postsynaptic). The postsynaptic distribution of CS synapses was studied electrophysiologically and through optical imaging, and the regression of CS axons was observed using conventional anterograde tracing as well as live imaging of CS neurons labeled using the exo utero electroporation technique.

Results

Developmental Redistribution of CS Synapses in Mice. Using WT C57BL/6 mice instead of rats, we reconstructed the in vitro CS projection system from our previous work (21) and compared the development of CS synapses in mice with that in rats (22). Coronal cortical and axial SpC slices (350 μm thick) were sectioned from postnatal day 0 (P0) mice, and the forelimb areas were dissected from the cortical sections. The slices were placed on a collagen-coated membrane and maintained at the liquid–gas interface (27). We then stimulated the deep layers of the cortical slices and recorded CS field EPSPs at 80-μm intervals along a lattice within the spinal gray matter. At 8 DIV, field EPSPs were recorded diffusely throughout the spinal gray matter, but their amplitude on the ventral side began to decline at 9 DIV and reached a minimum by 13 DIV (Fig. S1). This suggests CS syn-

Author contributions: T.O. and M.S. designed research; T.O., H.M., N.M., T.K., and N.Y. performed research; T.O., H.M., N.M., T.K., N.Y., M.M., and M.S. analyzed data; and T.O. and M.S. wrote the paper.

The authors declare no conflict of interest.

*This Direct Submission article had a prearranged editor.

[1]To whom correspondence should be addressed. E-mail: msakurai@med.teikyo-u.ac.jp.

This article contains supporting information online at www.pnas.org/lookup/suppl/doi:10.1073/pnas.0906551107/-/DCSupplemental.

apses were eliminated from the ventral side during that period. To examine changes in membrane potential during the CS EPSPs directly, we studied CS synaptic responses through optical imaging of voltage-sensitive dye (optical EPSP) (26) (Fig. S2*A*). Synaptic responses to cortical stimulation spread to the ventral area at 8 DIV, but peak responses in the ventral area of the SpC had declined by 13 DIV in the control cultures (Fig. S2*B*). It took about 1 d longer in mice than in rats to achieve diffuse transient synapse formation in the ventral areas, but the time course of the synapse elimination from the ventral side was about the same. Application of an NMDAR antagonist, 2-amino-5-phosphonopentanoic acid (APV, 50 μM) to the medium from 6 to 12 DIV blocked the elimination of ventral synapses, as we previously saw in cultures from rats (22, 23). Moreover, measurements of both field and optical EPSPs revealed that application of a 2B-selective blocker, ifenprodil (10 μM), prevented ventral synapse elimination to the same degree as APV (Figs. S1 and S2*B*).

To study the spatial distribution of CS axon terminals, we labeled CS axons through anterograde application of biocytin to the deep layers of the cortical slices 24 h before fixation (22). We found that in the control cultures, the axon terminals were widely distributed throughout the gray matter of the SpC at 8 DIV but had regressed from the ventral side by 13 DIV (Fig. S3). In cultures exposed to ifenprodil, however, the axon terminals continued to be distributed in the gray matter at 13 DIV, as was the case with APV (Fig. S3). These results suggest that 2B is crucially involved in the synapse elimination seen under control conditions. To confirm the 2B dependence of the CS synapse elimination, we next prepared the same slice cultures using $2b^{-/-}$ (20) and $2a^{-/-}$ (28) mice.

NMDA Component of CS Synapses in Cultured Slices from $2b^{-/-}$ Mice. Some studies have shown that there are no functional NMDAR channels in $2b^{-/-}$ cells in the hippocampus (20, 29). If NMDARs were eliminated from all neurons in $2b^{-/-}$ mutants, we would be unable to use these mice to study the specific involvement of 2B in synapse elimination. We therefore examined the contribution made by NMDARs to CS synaptic responses in the absence of the 2B subunit by coculturing slices from WT and $2b^{-/-}$ mice.

We first checked for the presence of the NMDA component in CS field EPSPs recorded from cultures of WT or $2b^{-/-}$ SpC in pharmacological blocking experiments. APV-sensitive components were detected in both WT and $2b^{-/-}$ SpC cultures in Mg-free medium containing 10 μM CNQX (Fig. 1*A*). The NMDA responses in $2b^{-/-}$ SpCs were greatly reduced by 100 nM NVP-AAM077, which is known to block the 2A subunit at low concentrations (unless otherwise stated, $n = 8$ and $P < 0.01$, Student's t test was used for statistical analyses; Fig. 1*B*). We then measured NMDA and AMPA CS-EPSCs in WT, $2b^{-/-}$, and $2a^{-/-}$ slices recorded in the whole-cell clamp configuration at holding potentials of −70 or +40 mV, respectively (Fig. 1*C*). Short-lasting NMDAR components were detected in the slices from $2b^{-/-}$ SpCs at 8 DIV. Averaged peak amplitudes and the areas underneath the NMDA currents were smaller in $2b^{-/-}$ than WT slices (500.6 ± 88.2 pA and 47.2 ± 19.5 pC in $2b^{-/-}$ slices; 881.7 ± 42.3 pA and 152.3 ± 23.7 pC in WT slices; $n = 6$; $P < 0.05$; Fig. 1*C*), and the averaged decay times were shorter in $2b^{-/-}$ than WT slices (62.1 ± 8.8 ms in $2b^{-/-}$ slices; 142.4 ± 8.6 ms in WT slices; $n = 6$; $P < 0.01$; Fig. 1*C*). In addition, the peak amplitudes of AMPA currents were larger in $2b^{-/-}$ than WT slices (780 ± 72.1 pA in $2b^{-/-}$ slices; 513.3 ± 66.6 pA in WT slices; $n = 6$; $P < 0.05$;

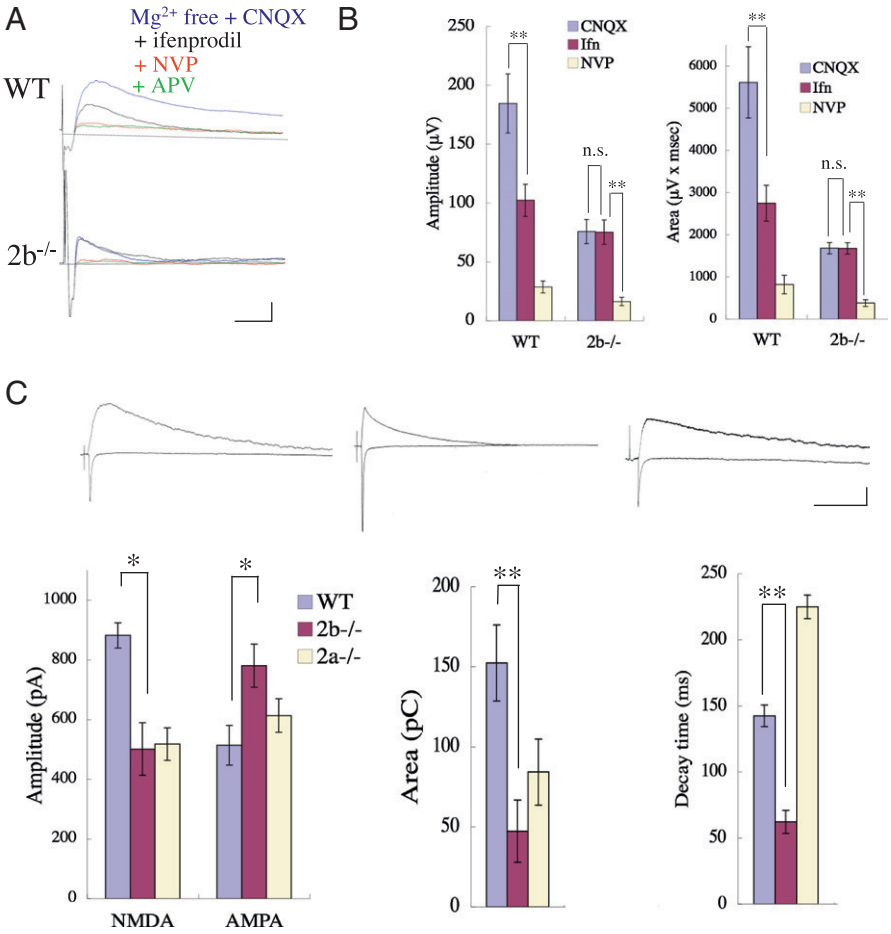

Fig. 1. NMDAR and non-NMDAR components of CS synaptic responses in WT, $2b^{-/-}$, and $2a^{-/-}$ mice. (*A*) Pharmacological study of CS field EPSPs at 8 DIV. Representative averaged traces before and 10 min after successive applications of CNQX, ifenprodil, NVP-AAM077, and APV in WT (*Upper*) and $2b^{-/-}$ SpC (*Lower*) slices. CS field EPSPs recorded in Mg-free medium with 10 μM CNQX were APV-sensitive and ifenprodil-insensitive in $2b^{-/-}$ mice. Calibration: 100 μV, 20 ms. (*B*) Averaged amplitudes (*Left*) and the areas underneath the field EPSPs (*Right*) after the application of CNQX, ifenprodil, and NVP-AAM077. (*C*) Whole-cell recordings of NMDAR- and AMPAR-mediated responses in SpC slices at 8 DIV. (*Upper*) Averaged CS EPSC traces recorded at holding potentials of +40 and −70 mV in WT (*Left*), $2b^{-/-}$ (*Center*), and $2a^{-/-}$ (*Right*) SpCs. Calibration: 200 pA, 100 ms. (*Lower*) Averaged amplitudes of NMDA and AMPA EPSCs (*Left*), the area underneath (*Center*), and decay times (*Right*) of NMDA EPSCs. *$P < 0.05$; **$P < 0.01$.

Fig. 1*C*). Taken together, these data indicate that robust functional NMDAR channels with shorter decay times, probably the 2A subtype, are present in CS synapses in $2b^{-/-}$ mice. By contrast, longer decay times were seen in $2a^{-/-}$ slices (225.0 ± 8.9 ms in $2a^{-/-}$ slices; $n = 6$; $P < 0.01$; Fig. 1*C*), although the current amplitudes were reduced to 517 ± 54.8 pA, which was about the same as the reduction in $2b^{-/-}$ slices. The area under the current was larger in $2a^{-/-}$ than $2b^{-/-}$ slices, however (84.1 ± 20.7 pC; $n = 6$). There was no significant difference in the AMPA receptor response between WT and $2a^{-/-}$ slices (513.3 ± 66.6 pA in $2a^{-/-}$).

CS Synapse Elimination in $2b^{-/-}$ and $2a^{-/-}$ Mice. In presynaptic neurons, the 2B subunit is found in the somata and in axon terminals, and it may play an essential role in synaptic reorganization (30–34) (*Discussion*). To assess the 2B dependence of CS synapse elimination and determine whether elimination is dependent on NMDAR activation in cortical cells (presynaptic) or SpC cells (postsynaptic), we cocultured slices obtained from WT and $2b^{-/-}$ mice (heterotypic coculture) and studied the developmental redistribution of CS synapses (Fig. S4*A*). In the following descriptions of experiments using heterotypic cocultures, the origin of the slices used for the Cx will be written before those used for the SpC (e.g., a cocultured pair consisting of a cortical slice from a WT mouse and an SpC slice from a $2b^{-/-}$ mouse will be written as WT-$2b^{-/-}$).

Electrophysiological Study of CS Field EPSPs. The reduction of the mean amplitudes of field EPSPs normally seen in the ventral area of the SpC during the period from 8 to 13 DIV was blocked when SpC slices were prepared from $2b^{-/-}$ mice (WT-$2b^{-/-}$ pairs) (Fig. S4 *B* and *C*). On the other hand, the ventral reduction in mean EPSP amplitude was unaffected when SpC slices were obtained from $2a^{-/-}$ mice (WT-$2a^{-/-}$ pairs) (Fig. S4 *B* and *C*). This indicates that 2A is not essential for CS synapse elimination in this system. The ventral reduction in mean EPSP amplitude was also observed when $2b^{-/-}$ mice were used for the cortical slices ($2b^{-/-}$-WT pairs) (Fig. S4 *B* and *C*), which suggests that cortical (presynaptic) 2B is not responsible for the observed ventral synapse elimination.

Optical Recordings of CS EPSPs. We next used a voltage-sensitive dye to record optical EPSPs to measure and visualize the spatial distribution of CS-EPSPs in the SpC directly (26). Fig. 2*A* shows the distribution of optical EPSPs recorded 11 ms after cortical stimulation, at a time when the signal intensity had reached its peak in this ventral region of interest (ROI). In WT pairs, the amplitudes of the optical EPSPs declined in ventral areas during the period from 8 to 13 DIV, whereas almost no change was seen in the WT-$2b^{-/-}$ pairs (Fig. 2*B Left*). As with control pairs, optical EPSPs in the ventral areas had substantially declined in WT-$2a^{-/-}$ pairs by 13 DIV (Fig. 2*B Center*). Likewise, optical EPSPs recorded from $2b^{-/-}$-WT pairs showed reductions in ventral areas that were similar to those seen with WT pairs (Fig. 2*B Right*). For quantitative analysis, we selected dorsal and ventral ROIs (Fig. 2*A Inset*) and compared the ventrodorsal ratios of the averaged peak amplitudes of optical EPSPs. This ratio declined during the period from 8 to 13 DIV in WT pairs (0.42 ± 0.01–0.23 ± 0.02; $n = 8$; $P < 0.05$; Fig. 2*C*) but did not decline in WT-$2b^{-/-}$ pairs during the same period (0.41 ± 0.01–0.42 ± 0.03; $n = 10$; $P > 0.5$; Fig. 2*C*). Like the WT pairs, both the WT-$2a^{-/-}$ and $2b^{-/-}$-WT pairs showed reductions in their ventrodorsal ratios [$2b^{-/-}$-WT pairs (0.45 ± 0.03–0.33 ± 0.03; $n = 10$; $P < 0.05$) and WT-$2b^{-/-}$ pairs (0.50 ± 0.02–0.37 ± 0.01; $n = 10$; $P < 0.05$)] (Fig. 2*C*). Our studies of CS field EPSPs and CS optical EPSPs both suggest that 2A is not essential for the synapse elimination seen during development and that 2B in the Cx (presynaptic 2B) is not necessary either.

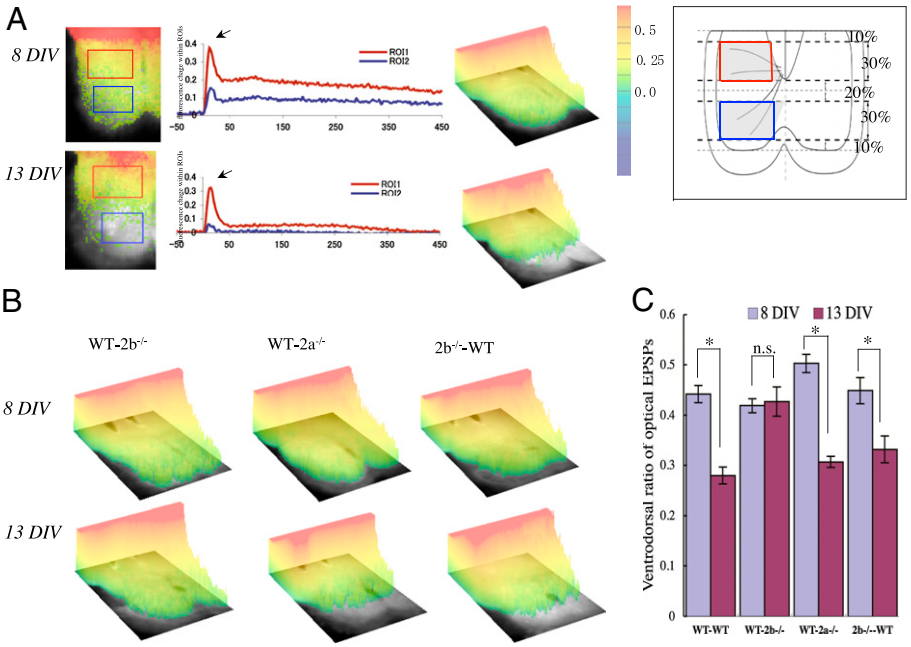

Fig. 2. Developmental changes in the spatial distribution of optical EPSPs. (*A*) Spatial and temporal patterns of synaptic responses in the SpC at 8 and 13 DIV in WT cocultures recorded 11 ms after cortical stimulation. The pseudocolored optical images are superimposed on the hemi-SpC. (*Center*) Fluorescence changes within ROIs in the dorsal and ventral areas are shown. Arrows indicate the times at which images were recorded. The pseudocolor bar indicates signal intensity [percent fractional change in normalized fluorescence (%ΔF/F)]. (*Inset*) Schematic drawing showing the selection of ROIs in the dorsal (boxed by red line) and ventral (boxed by blue line) areas. Spatial patterns of peak synaptic responses (*B*) and ventrodorsal ratios of optical EPSPs (*C*) in the indicated culture pairs at 8 and 13 DIV. In *B*, we set the upper cutoff level of the signal intensity just above the maximum intensity of the SpC signal and trimmed the cortical part to a degree that provided a margin of safety. n.s., Not significant. *$P < 0.05$.

Anterograde Labeling of CS Axons. In WT-$2b^{-/-}$ pairs, CS axon terminals labeled with biocytin continued to be widely distributed in the gray matter of the SpC at 13 DIV (Fig. S5 *A* and *B*). By contrast, CS axon terminals on the ventral side were largely eliminated by 13 DIV in WT-$2a^{-/-}$ and $2b^{-/-}$-WT pairs (Fig. S5 *A* and *B*). The ventrodorsal ratio of CS fiber densities declined between 8 and 13 DIV in WT-$2a^{-/-}$ and $2b^{-/-}$-WT pairs but not in WT-$2b^{-/-}$ pairs (Fig. S5*C*). The regression of CS axons from the ventral area was blocked when $2b^{-/-}$ mice were used for the SpC slices but not when $2a^{-/-}$ mice were used for the SpC slices or when $2b^{-/-}$ mice were used for the cortical slices.

Live Imaging of CS Axons in the Same Cultures. In addition to comparing the distributions of CS axons among groups using fixed tissues (cocultures), we followed the distribution of CS axons in single living cocultures. To label the cortical neurons of layer V, we used exo utero electroporation to transfect an enhanced yellow fluorescent protein (EYFP) expression vector into the Cx during the period extending from embryonic day (E) 12.5 to E13.5 (35, 36). Thereafter, cortical slices expressing EYFP were cocultured heterotypically with SpC slices from WT, $2b^{-/-}$, or $2a^{-/-}$ mice (Fig. 3*A*; details presented in *SI Materials and Methods*), and regression of the axon terminals was observed.

To compare the spatial distribution of CS axon terminals and CS synaptic activity, we assessed the correlation between EYFP fluorescence intensity (fiber density) and optical EPSP amplitude (CS synaptic activity) in a 4×4 lattice-like pattern of ROIs (26). Mean EYFP fluorescence intensity increased monotonically with optical EPSP amplitude, and the Spearman's rank correlation coefficient relating the two was 0.85 ($n = 5$; $P < 0.001$; Fig. 3*B*). This correlation between the presence of CS fibers and optical EPSP amplitude suggests that most cortical fibers that entered the SpC made synapses at relatively even intervals along their trajectories.

When recording images of EYFP fluorescence, we minimized phototoxicity by taking pictures at only two time points: 8 DIV and 13 DIV. In the first view, axon terminals in all the cultures can be seen to extend nearly to the ventral edge of the SpC slice (Fig. 3*C Upper*). In the second view, however, axons had largely regressed from the ventral sides of SpC slices from WT or $2a^{-/-}$ mice, whereas most of the ventral axons survived in SpC slices from $2b^{-/-}$ mice (Fig. 3*C Lower*). Mean fluorescence intensities in the ventral ROIs (Fig. 2*A Inset*) diminished between 8 and 13 DIV in WT SpCs (mean intensities of the dorsal vs. ventral ROIs at 8 DIV: 28.4 ± 7.4 vs. 18.0 ± 5.2; at 13 DIV: 23.6 ± 3.8 vs. 6.4 ± 1.9; $n = 12$) and $2a^{-/-}$ SpCs (intensities of the dorsal vs. ventral at 8 DIV: 38.1 ± 7.2 vs. 26.4 ± 5.6; at 13 DIV: 34.2 ± 7.2 vs. 12.9 ± 3.3; $n = 6$). By contrast, the intensities in the ventral ROIs did not change significantly in the $2b^{-/-}$ SpCs (intensities of the dorsal vs. ventral at 8 DIV: 31.3 ± 9.3 vs. 21.5 ± 7.0; at 13 DIV: 27.2 ± 9.1 vs.

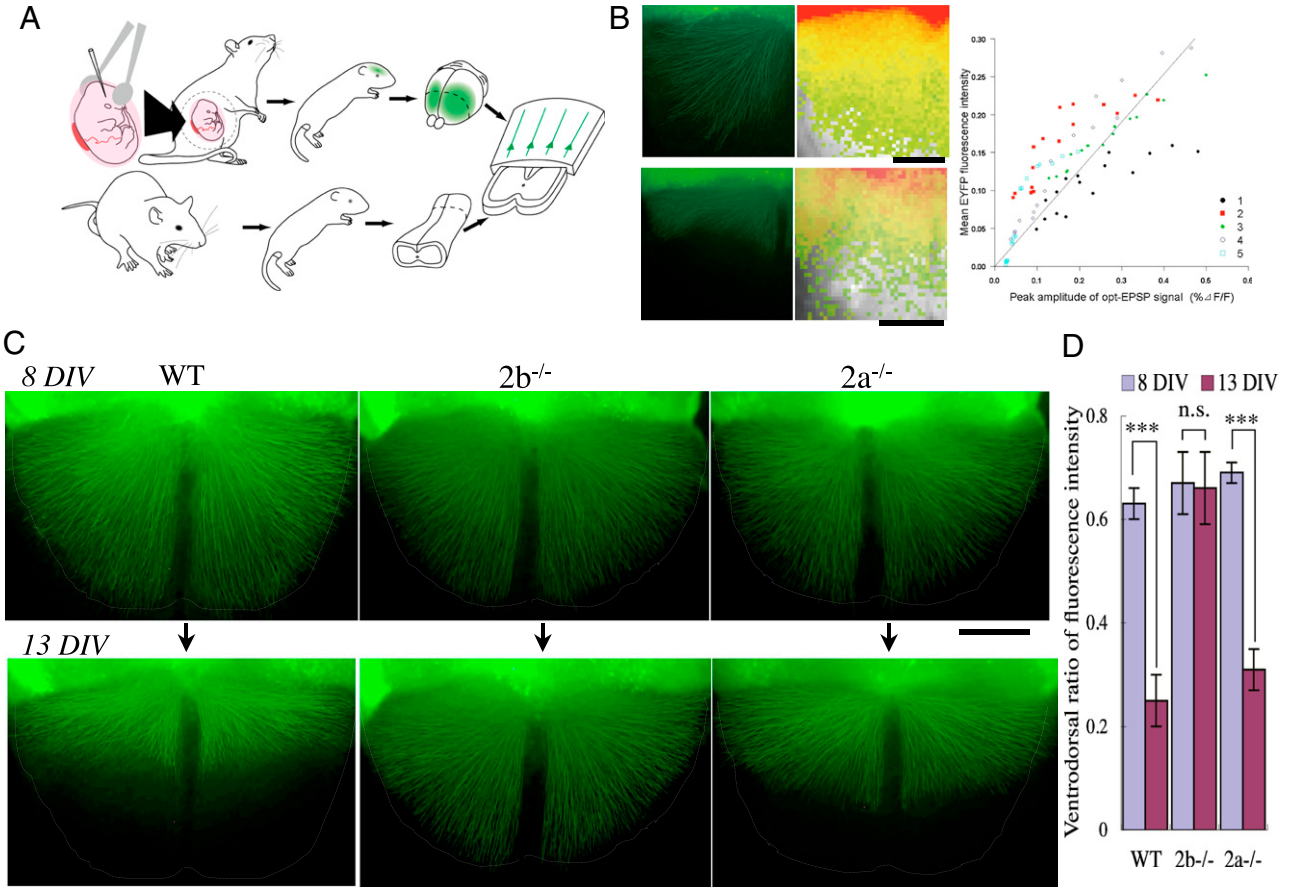

Fig. 3. Live imaging of CS axons. (*A*) Schematic drawings of exo utero electroporation of an EYFP expression vector into CS projection neurons and the heterotypic coculture of cortical and SpC slices derived from animals with different genotypes. (*B*) Distribution of labeled CS axons and optical EPSPs observed in the same cocultures. (*Left*) Spatial distribution of EYFP-labeled CS axons coincided with areas in which larger amplitude optical EPSPs were recorded, which is indicative of the distribution of CS synapses. (*Right*) Peak amplitudes of optical EPSPs are plotted against EYFP fluorescence intensity (fiber density of labeled cortical efferent axons) in 16 ROIs from five slices. The Spearman's rank correlation coefficient relating the two was 0.85 ($n = 5$; $P < 0.001$). (Scale bar: 200 μm.) (*C*) Images of CS axons in coculture with WT (*Left*), $2b^{-/-}$ (*Center*), or $2b^{-/-}$ (*Right*) SpCs. The first view was taken at 8 DIV, and the second view was taken at 13 DIV. (Scale bar: 250 μm.) (*D*) Ventrodorsal ratios of averaged intensities in the first and second views. n.s., not significant. ***$P < 0.001$.

18.5 ± 7.5; $n = 8$). Ventrodorsal ratios of mean fluorescence intensities declined between 8 and 13 DIV in WT and $2a^{-/-}$ SpCs, but the ratio was unchanged in $2b^{-/-}$ SpCs (Fig. 3*D*). Thus, our observations of CS axons in living cocultures verified that axonal regression associated with synapse elimination occurred when SpCs were derived from $2a^{-/-}$ mice but not when they were derived from $2b^{-/-}$ mice.

Effect of Manipulating Ca^{2+} Entry Through NMDAR on the Synapse Elimination. We compared the effects of nonselective blockade of 2A and 2B by APV with those of selective blockade of 2B by ifenprodil on synapse elimination in WT slices (37, 38). We first examined the dose-inhibition relationship for field EPSP amplitude and found that 2.5 μM APV blocked NMDAR-mediated field EPSPs to a degree comparable to 10 μM ifenprodil (Fig. S6*A*). At these doses, the blockade produced by the two antagonists had similar inhibitory effects on peak amplitudes and areas under the NMDAR EPSCs (Fig. S6*B*). If this concentration of APV does not block synapse elimination, 2A/2B divergence cannot be explained by a quantitative difference in Ca^{2+} influx through these channels. However, we found that 2.5 μM APV blocked CS axonal regression to nearly the same degree as ifenprodil (Fig. S6 *C*). This might reflect the fact that 2B is the dominant NMDA at this stage in WT mice, such that the vast majority of NMDARs blocked by APV should also be 2B. We then partially blocked the putative 2B-mediated CS EPSC in $2a^{-/-}$ slices so that Ca^{2+} entry through CS synapses in $2a^{-/-}$ slices was reduced to the same level as in $2b^{-/-}$ slices. Because the areas under the NMDA currents in $2b^{-/-}$ were about 44% smaller than those in $2a^{-/-}$ (Fig. 1*C*), we treated the $2a^{-/-}$ slices with 2 μM ifenprodil, which reduced NMDA currents by about 45% (Fig. S7 *A* and *B*). Although we expect this would reduce Ca^{2+} entry through CS synapses to a level similar to that seen in $2b^{-/-}$ slices, ventral elimination was not blocked (Fig. S7*C*).

Discussion

Because $2b^{-/-}$ mice lack a suckling reflex, it is difficult to keep them alive for longer than 24 h. This had impeded the study of 2B function and NMDAR expression during development, although the NMDA response was found to be totally absent in the hippocampal CA1 region of $2b^{-/-}$ mice kept alive until P3 through artificial feeding (20). Moreover, selective KO of 2B in hippocampal CA3 pyramidal cells virtually eliminated NMDA-mediated currents at CA3 synapses (29). These results imply that the 2B NMDAR subunit expressed during early development might regulate the expression of other NMDAR subunits in the postsynaptic membrane. However, we recorded robust NMDAR-mediated synaptic currents in SpC slices from $2b^{-/-}$ mice at 7 DIV, and their rapid deactivation kinetics were consistent with 2A subunit-mediated currents (7, 8) (Fig. 1*B*). These findings indicate that 2B is not required for the trafficking of NMDARs to the postsynaptic membrane in the SpC and that AMPA currents are increased in the SpC of $2b^{-/-}$ mice (Fig. 1*B*), which is consistent with the results obtained with dissociated cortical neurons prepared from $2b^{-/-}$ mice (39).

Presynaptic activity is also known to play an important role in developmental plasticity, including the Ca^{2+} waves involved in retinotopic mapping in the superior colliculus and visual Cx (30, 31). 2B receptors may play a key role in generating or modulating such presynaptic activity. It was also recently shown that 2B-containing NMDARs are present in the presynaptic terminals that modulate synaptic activity (34) and play an essential role in the induction of long-term depression (LTD) (32, 33), which suggests their possible involvement in synapse elimination. In our heterotypic cocultures, both synapse elimination and axonal regression persisted when the Cx slices were from $2b^{-/-}$ mice. This suggests that the presence of the 2B subunit on the presynaptic side is not essential for activity-dependent synapse elimination.

Whether or not NMDAR subpopulations are differentially involved in synaptic plasticity is a long-running controversy. Some studies have shown that 2A and 2B are selectively involved in long-term potentiation (LTP) and LTD at synapses in hippocampal CA1 (38, 40, 41) and the juvenile superior colliculus (42), whereas others suggest there is an absence of NMDAR subtype selectivity in hippocampal LTP (43), or that LTD at synapses in hippocampal CA1 is independent of 2B (44). There are also apparent discrepancies in the data on the roles played by 2B and 2A in the developmental plasticity of synapse formation in different brain areas. Overall, however, it appears that the contribution made by 2B to synaptic currents tends to decline during development, whereas there is a corresponding increase in the contribution made by 2A. The levels of mRNA and protein expression are also indicative of a developmental switch from 2B to 2A (5, 6), and it has been suggested that this replacement of 2B by 2A during postnatal development is linked to the ability of neuronal circuits to exhibit synaptic plasticity (13, 14). For instance, changes in the subunit composition of NMDARs from 2B to 2A correlate with the end of the critical period for LTP (9–12), whereas the critical period for synaptic plasticity in the barrel Cx appears to be independent of changes in NMDAR subunit composition (19). To determine whether 2B is selectively involved in CS synapse elimination and to assess the respective involvement of 2A and 2B in developmental plasticity, it is necessary to use both $2a^{-/-}$ and $2b^{-/-}$ mice. Our finding that synapse elimination and axonal regression on the ventral side were blocked in SpC slices from $2b^{-/-}$ mice but not $2a^{-/-}$ mice means that distinct subpopulations of NMDARs contribute to at least some types of synapse rearrangement during early development.

How different NMDAR subunits can produce different forms of plasticity remains unknown. Because of its slower kinetics, 2B mediates greater influx of Ca^{2+} into postsynaptic cells (7, 8). Consequently, the net charge through NMDARs was 2-fold larger in $2a^{-/-}$ than $2b^{-/-}$ slices at a holding potential of +40 mV in whole-cell recordings of CS-EPSCs (Fig. 1*C*). Thus, one possible explanation for our present findings is that they reflect crucial differences in the total Ca^{2+} influx through 2B and 2A channels that result from their differing kinetics. This difference in Ca^{2+} influx could, in turn, lead to activation of different signaling pathways, because large increases in Ca^{2+} predominantly activate kinases causing LTP, whereas moderate increases activate phosphatases causing LTD (45–47). Alternatively, the intracellular signaling cascades downstream of 2B-mediated Ca^{2+} entry may differ from those mediated by other NMDAR subtypes (12, 48–51); moreover, they might be specifically related to synapse elimination. In thalamocortical synapses, for example, although the shift from 2B to 2A is associated with the end of the critical period, this does not reflect a difference in their kinetics, which makes it difficult to explain their plasticity based only on total Ca^{2+} influx (51). In the present study, ventral synapse elimination in $2a^{-/-}$ was not blocked, even when the net charge through NMDARs (putative 2B) in $2a^{-/-}$ was reduced to the same level as (putative 2A) in $2b^{-/-}$. The selective involvement of the 2B-NMDAR in ventral synapse elimination is difficult to explain based solely on greater Ca^{2+} entry through 2B-NMDAR channels. The result might favor the possibility that Ca^{2+} entry through 2B-NMDARs and 2A-NMDARs activates different intracellular signaling cascades.

Materials and Methods

Methods for organotypic slice culture, electrophysiological study, optical recordings, and anterograde labeling are described in detail in *SI Materials and Methods*.

Heterotypic Cocultures Using KO Animals. Mutant mice lacking the 2B subunit were produced by homologous recombination by Kutsuwada et al. (20). Heterozygous $2b^{+/-}$ mice were used for breeding, because mice lacking

both 2B alleles die soon after birth. The 2B mutant mice were successively backcrossed with C57BL/6 mice for more than 15 generations to yield homozygous mutant mice ($2b^{-/-}$) with a pure C57BL/6 genetic background. Genotypes were determined by genomic PCR from tail clippings. Homozygous mutant mice lacking the 2A subunit ($2a^{-/-}$) with a C57BL/6 background (28) were bred and maintained at the Teikyo University School of Medicine. Using these animals, we prepared three types of heterotypic slice cocultures (Fig. S4*A*). In addition, for the live imaging experiments summarized in Fig. 3*C*, cortical slices were prepared from ICR mice, whose cortical neurons express EYFP. SpC slices were obtained from WT, $2b^{-/-}$, and $2a^{-/-}$ mice.

Exo Utero Electroporation and Live Imaging. To label cortical neurons, an EYFP expression vector (pCAGGS-EYFP; a gift from H. Niwa, RIKEN, Kobe, Japan) was transfected to E12.5 or E13.5 embryos by electroporation with exo utero manipulation (35, 36). The pups were recovered by caesarean section on E19.5 and immediately subjected to slice culture. Live imaging was carried out using an upright epifluorescence microscope (Eclipse E800; Nikon). Details of exo utero electroporation and quantitative evaluation of the fluorescence intensity of the dorsal and ventral areas are presented in *SI Materials and Methods*.

ACKNOWLEDGMENTS. We thank Dr. Tetsuichiro Saito (University of Chiba) for his technical advice on exo utero electroporation. We thank Dr. Hitoshi Niwa (RIKEN) for kindly supplying pCAGGS promoter. We also thank Dr. Issei Kurahashi (University of Tokyo) for his help with the statistical analysis. This work was supported by Grants-in-Aid to M.S. (Grant 20300138) and T.O. (Grant 20800047) and a grant for Scientific Research on Priority Areas (Grant 18021034) to M.S. from the Ministry of Education, Culture, Sports, Science, and Technology, Japan.

1. Kleinschmidt A, Bear MF, Singer W (1987) Blockade of "NMDA" receptors disrupts experience-dependent plasticity of kitten striate cortex. *Science* 238:355–358.
2. Cline HT, Constantine-Paton M (1989) NMDA receptor antagonists disrupt the retinotectal topographic map. *Neuron* 3:413–426.
3. Fox K, Schlaggar BL, Glazewski S, O'Leary DD (1996) Glutamate receptor blockade at cortical synapses disrupts development of thalamocortical and columnar organization in somatosensory cortex. *Proc Natl Acad Sci USA* 93:5584–5589.
4. Iwasato T, et al. (1997) NMDA receptor-dependent refinement of somatotopic maps. *Neuron* 19:1201–1210.
5. Sheng M, Cummings J, Roldan LA, Jan YN, Jan LY (1994) Changing subunit composition of heteromeric NMDA receptors during development of rat cortex. *Nature* 368:144–147.
6. Liu XB, Murray KD, Jones EG (2004) Switching of NMDA receptor 2A and 2B subunits at thalamic and cortical synapses during early postnatal development. *J Neurosci* 24: 8885–8895.
7. Flint AC, Maisch US, Weishaupt JH, Kriegstein AR, Monyer H (1997) NR2A subunit expression shortens NMDA receptor synaptic currents in developing neocortex. *J Neurosci* 17:2469–2476.
8. Vicini S, et al. (1998) Functional and pharmacological differences between recombinant N-methyl-D-aspartate receptors. *J Neurophysiol* 79:555–566.
9. Carmignoto G, Vicini S (1992) Activity-dependent decrease in NMDA receptor responses during development of the visual cortex. *Science* 258:1007–1011.
10. Hestrin S (1992) Developmental regulation of NMDA receptor-mediated synaptic currents at a central synapse. *Nature* 357:686–689.
11. Erisir A, Harris JL (2003) Decline of the critical period of visual plasticity is concurrent with the reduction of NR2B subunit of the synaptic NMDA receptor in layer 4. *J Neurosci* 23:5208–5218.
12. Barria A, Malinow R (2005) NMDA receptor subunit composition controls synaptic plasticity by regulating binding to CaMKII. *Neuron* 48:289–301.
13. Espinosa JS, Wheeler DG, Tsien RW, Luo L (2009) Uncoupling dendrite growth and patterning: Single-cell knockout analysis of NMDA receptor 2B. *Neuron* 62:205–217.
14. Fagiolini M, et al. (2003) Separable features of visual cortical plasticity revealed by N-methyl-D-aspartate receptor 2A signaling. *Proc Natl Acad Sci USA* 100:2854–2859.
15. Quinlan EM, Philpot BD, Huganir RL, Bear MF (1999) Rapid, experience-dependent expression of synaptic NMDA receptors in visual cortex in vivo. *Nat Neurosci* 2:352–357.
16. Roberts EB, Ramoa AS (1999) Enhanced NR2A subunit expression and decreased NMDA receptor decay time at the onset of ocular dominance plasticity in the ferret. *J Neurophysiol* 81:2587–2591.
17. Heinrich JE, Singh TD, Sohrabji F, Nordeen KW, Nordeen EJ (2002) Developmental and hormonal regulation of NR2A mRNA in forebrain regions controlling avian vocal learning. *J Neurobiol* 51:149–159.
18. Philpot BD, Cho KK, Bear MF (2007) Obligatory role of NR2A for metaplasticity in visual cortex. *Neuron* 53:495–502.
19. Lu HC, Gonzalez E, Crair MC (2001) Barrel cortex critical period plasticity is independent of changes in NMDA receptor subunit composition. *Neuron* 32:619–634.
20. Kutsuwada T, et al. (1996) Impairment of suckling response, trigeminal neuronal pattern formation, and hippocampal LTD in NMDA receptor epsilon 2 subunit mutant mice. *Neuron* 16:333–344.
21. Takuma H, Sakurai M, Kanazawa I (2002) *In vitro* formation of corticospinal synapses in an organotypic slice co-culture. *Neuroscience* 109:359–370.
22. Ohno T, Maeda H, Sakurai M (2004) Regionally specific distribution of corticospinal synapses because of activity-dependent synapse elimination in vitro. *J Neurosci* 24:1377–1384.
23. Ohno T, Sakurai M (2005) Critical period for activity-dependent elimination of corticospinal synapses in vitro. *Neuroscience* 132:917–922.
24. Kamiyama T, Yoshioka N, Sakurai M (2006) Synapse elimination in the corticospinal projection during the early postnatal period. *J Neurophysiol* 95:2304–2313.
25. Martin JH, Friel KM, Salimi I, Chakrabarty S (2009) *Developmental Neurobiology*, ed Lemke G (Elsevier, Amsterdam), pp 403–414.
26. Maeda H, Ohno T, Sakurai M (2007) Optical and electrophysiological recordings of corticospinal synaptic activity and its developmental change in in vitro rat slice cocultures. *Neuroscience* 150:829–840.
27. Yamamoto N, Kurotani T, Toyama K (1989) Neural connections between the lateral geniculate nucleus and visual cortex in vitro. *Science* 245:192–194.
28. Sakimura K, et al. (1995) Reduced hippocampal LTP and spatial learning in mice lacking NMDA receptor epsilon 1 subunit. *Nature* 373:151–155.
29. Akashi K, et al. (2009) NMDA receptor GluN2B (GluR epsilon 2/NR2B) subunit is crucial for channel function, postsynaptic macromolecular organization, and actin cytoskeleton at hippocampal CA3 synapses. *J Neurosci* 29:10869–10882.
30. Wong RO (1999) Retinal waves and visual system development. *Annu Rev Neurosci* 22:29–47.
31. McLaughlin T, Torborg CL, Feller MB, O'Leary DD (2003) Retinotopic map refinement requires spontaneous retinal waves during a brief critical period of development. *Neuron* 40:1147–1160.
32. Casado M, Isope P, Ascher P (2002) Involvement of presynaptic N-methyl-D-aspartate receptors in cerebellar long-term depression. *Neuron* 33:123–130.
33. Lien CC, Mu Y, Vargas-Caballero M, Poo MM (2006) Visual stimuli-induced LTD of GABAergic synapses mediated by presynaptic NMDA receptors. *Nat Neurosci* 9:372–380.
34. Jourdain P, et al. (2007) Glutamate exocytosis from astrocytes controls synaptic strength. *Nat Neurosci* 10:331–339.
35. Saito T, Nakatsuji N (2001) Efficient gene transfer into the embryonic mouse brain using in vivo electroporation. *Dev Biol* 240:237–246.
36. Saito T (2006) *In vivo* electroporation in the embryonic mouse central nervous system. *Nat Protoc* 1:1552–1558.
37. Yoshimura Y, Ohmura T, Komatsu Y (2003) Two forms of synaptic plasticity with distinct dependence on age, experience, and NMDA receptor subtype in rat visual cortex. *J Neurosci* 23:6557–6566.
38. Liu L, et al. (2004) Role of NMDA receptor subtypes in governing the direction of hippocampal synaptic plasticity. *Science* 304:1021–1024.
39. Hall BJ, Ripley B, Ghosh A (2007) NR2B signaling regulates the development of synaptic AMPA receptor current. *J Neurosci* 27:13446–13456.
40. Hrabetova S, et al. (2000) Distinct NMDA receptor subpopulations contribute to long-term potentiation and long-term depression induction. *J Neurosci* 20:RC81.
41. Massey PV, et al. (2004) Differential roles of NR2A and NR2B-containing NMDA receptors in cortical long-term potentiation and long-term depression. *J Neurosci* 24:7821–7828.
42. Zhao JP, Constantine-Paton M (2007) $NR2A^{-/-}$ mice lack long-term potentiation but retain NMDA receptor and L-type Ca^{2+} channel-dependent long-term depression in the juvenile superior colliculus. *J Neurosci* 27:13649–13654.
43. Berberich S, et al. (2005) Lack of NMDA receptor subtype selectivity for hippocampal long-term potentiation. *J Neurosci* 25:6907–6910.
44. Morishita W, et al. (2007) Activation of NR2B-containing NMDA receptors is not required for NMDA receptor-dependent long-term depression. *Neuropharmacology* 52:71–76.
45. Artola A, Bröcher S, Singer W (1990) Different voltage-dependent thresholds for inducing long-term depression and long-term potentiation in slices of rat visual cortex. *Nature* 347:69–72.
46. Lisman J (1989) A mechanism for the Hebb and the anti-Hebb processes underlying learning and memory. *Proc Natl Acad Sci USA* 86:9574–9578.
47. Mizuno T, Kanazawa I, Sakurai M (2001) Differential induction of LTP and LTD is not determined solely by instantaneous calcium concentration: An essential involvement of a temporal factor. *Eur J Neurosci* 14:701–708.
48. Sheng M, Kim MJ (2002) Postsynaptic signaling and plasticity mechanisms. *Science* 298:776–780.
49. Sans N, et al. (2000) A developmental change in NMDA receptor-associated proteins at hippocampal synapses. *J Neurosci* 20:1260–1271.
50. Yoshii A, Sheng MH, Constantine-Paton M (2003) Eye opening induces a rapid dendritic localization of PSD-95 in central visual neurons. *Proc Natl Acad Sci USA* 100: 1334–1339.
51. Barth AL, Malenka RC (2001) NMDAR EPSC kinetics do not regulate the critical period for LTP at thalamocortical synapses. *Nat Neurosci* 4:235–236.